Preprint
UCRL-JC-140617

Transport Simulations for Tokamak Edge-Plasmas

T.D. Rognlien, R.H. Cohen, L.L. LoDestro, G.D. Porter, M.E. Rensink, D.D. Ryutov, and X.Q. Xu

This article was submitted to the
18th International Atomic Energy Agency Fusion Energy Conference,
Sorrento, Italy, October 4 – 10, 2000

September 27, 2000

U.S. Department of Energy
Lawrence Livermore National Laboratory

Transport Simulations for Tokamak Edge-Plasmas

T.D. Rognlien, R.H. Cohen, L.L. LoDestro, G.D. Porter, M.E. Rensink, D.D. Ryutov, and X.Q. Xu

University of California Lawrence Livermore National Laboratory,
Livermore, CA 94551, USA

e-mail contact of main author: trognlien@llnl.gov

Abstract. The edge plasma plays key roles in tokamak devices: generates the edge transport-barrier yielding the L-H core confinement transition, distributes the core charged-particle energy to surrounding material surfaces, shields the core from impurities, and removes helium ash in fusion plasmas. The transport of density, momentum, and energy in the near-separatrix edge region, and the corresponding self-consistent electrostatic potential, require a two-dimensional description, here incorporated into the UEDGE code. In the direction across the B-field, both turbulent transport and classical cross-field flows are important. The role of classical flows is analyzed in detail in the presence of an assumed diffusive turbulent transport. Results and explanations are given for the generation of radial electric field near the separatrix, edge plasma asymmetries and differences between double-null DIII-D and NSTX devices, comparisons with DIII-D diagnostics for single-null divertor, and core/edge transport coupling.

1. Introduction

Edge plasmas provide the interface between hot core plasmas and the material surfaces of the vacuum vessel in fusion energy devices. Understanding characteristics of the edge plasma is important both for predicting particle and heat fluxes onto the surfaces and for influencing the behavior of the core plasma. An example of the latter is the edge transport barrier of the L-H confinement transition for tokamaks, where the edge plasma supports a high edge temperature [1].

In recent years, substantial progress has been made in modeling two major aspects of edge plasma transport in tokamaks: classical drifts across the magnetic field, $\mathbf{B}$, (*e.g*, [2, 3, 4, 5, 6]) and plasma turbulence (*e.g.*, [7]). Here we focus on new developments in understanding cross-field drifts in the presence of assumed turbulent transport; a second paper at this conference focuses on advances in understanding the plasma turbulence and its effect on transport [8]. In this paper, Sec. 2. identifies key mechanisms for radial electric field (E_r) generation, Sec. 3. gives edge plasmas for double-null DIII-D [9] and NSTX [10] configurations, Sec. 4. compares experimental measurements with a detailed DIII-D single-null case, and Sec. 5. discusses progress with core/edge transport coupling. Conclusions are given within each section.

2. Processes determining E_r

The radial electric field in the plasma edge is of particular interest because its radial gradient gives rise to a shear in the poloidal $\mathbf{E}\times\mathbf{B}/B^2$ velocity that is believed to play an important role forming the edge transport barrier by suppressing edge turbulence [1]. Previous simulations [2, 3] show that a strong negative E_r typically forms just inside the magnetic separatrix as is often observed experimentally [1]. Analysis of these type of

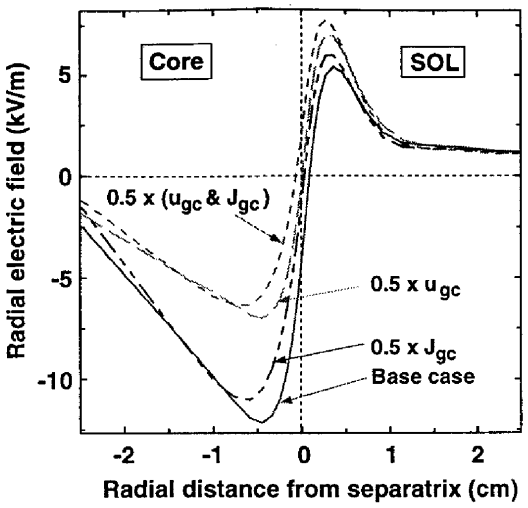

FIG. 1: Radial electric field at outer mid-plane for DIII-D simulation showing effects of changes to guiding-center drifts in Eq. (1).

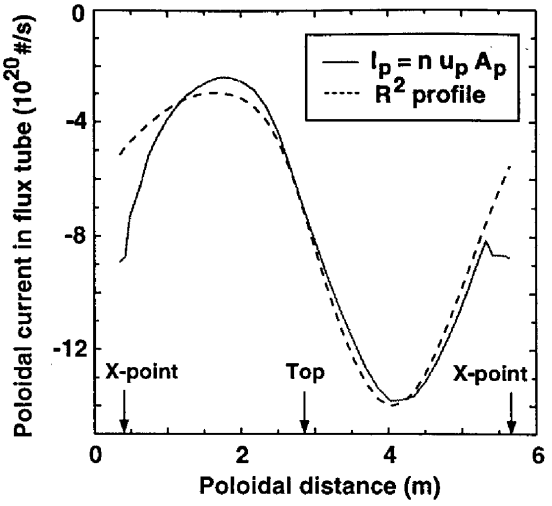

FIG. 2: Poloidal variation of particle current of flux tube of area A_p just inside the separatrix. R is the major radius.

simulations shows that the strongly negative E_r can be understood by considering only the particle and current continuity equations:

$$\nabla \cdot (n\mathbf{u}) = 0, \text{ and } \nabla \cdot \mathbf{J} = 0 \tag{1}$$

where n is the plasma density, $\mathbf{u}$ is the ion velocity, and $\mathbf{J}$ is the plasma current. Since $\mathbf{J}$ depends directly on the potential, ϕ, the second equation is often viewed as a relation for ϕ. Details of the UEDGE implementation of these equations are given in Ref. [3]. For tokamak edge plasma, key components in these equations are the poloidal velocity $u_E = E_r/B_t$ (toroidal field $B_t \approx B$) and the radial component of guiding-center velocity, $\mathbf{u}_{gc}$, and current, $\mathbf{J}_{gc}$, dominated by the ∇B and curvature drifts $\mathbf{u}_{gb}$. For these cases, the contribution of the parallel velocity ($u_{||}$) to the poloidal velocity is substantially less than u_E, but it can be added to the analysis.

Figure 1 shows the calculated E_r for the DIII-D single-null tokamak configuration at 3MW for four cases: a base-case, a case where both $\mathbf{u}_{gc}$, $\mathbf{J}_{gc}$ are reduced by a factor of 0.5 , and two cases where $\mathbf{u}_{gc}$, $\mathbf{J}_{gc}$ are separately reduced by 0.5. The nearly 50% reduction in $|E_r|$ is seen to be caused predominantly by the $\mathbf{u}_{gc}$ in the ion continuity equation. The plasma density, temperatures, and $u_{||}$ vary little between these four cases. The insensitivity of the current continuity condition to changes in $\mathbf{J}_{gc}$ is because the compensating parallel electron current is determined from the electron parallel momentum equation, where the comparatively large pressure and electric field terms nearly cancel owing to the large electron conductivity; thus, only small changes in the pressure or $E_{||}$ are needed to reduce $J_{||}$ by 50% to balance the reduction in $\mathbf{J}_{gc}$. The change in E_r is primarily controlled by the particle continuity condition. Here the change in the poloidally varying radial density flux from $\mathbf{u}_{gc}$ must be closed by an increase in the poloidal flux. The poloidal flux is controlled by u_E, and its variation can be simply understood as follows: Inside the separatrix, ϕ is nearly constant on a flux surface, giving $E_r \approx -\Delta\phi/\Delta r$ where Δr is the poloidally dependent separation of the flux surfaces. The ion continuity equation requires that the poloidal gradient of $I_p \equiv nu_E A_p = n(\Delta\phi/B\Delta r)2\pi R\Delta r = (2\pi n/B_0 R_0)\Delta\phi R^2$ be balanced by the radial gradient of $I_r \equiv nu_{gc,r}A_r$. Here $A_{p,r}$ are poloidal and radial areas of a flux

tube, and R is the major radius. Figure 2 confirms that $I_p \propto R^2$ inside the separatrix for the simulations in Fig. 1. The poloidal gradient of I_p (Fig. 2) has just the correct variation to match the dominantly vertical $\partial I_r/\partial r \sim -I_r/\ell_p$, where ℓ_p is the radial scale-length of ion pressure, nT_i. Thus, solving $\nabla \cdot (\mathbf{I}_p + \mathbf{I}_r) = 0$ inside the separatrix at the top of the machine yields

$$E_r \approx -0.5\mathcal{F}|u_{gb}B|(R_0/\ell_{p,t}) = -0.5\mathcal{F}v_t(\rho_i/\ell_{p,t}). \quad (2)$$

Here $\mathcal{F} = (\partial\psi/\partial r)/(\partial\psi/\partial r)_t$ with ψ being the poloidal flux and subscript t denoting the top of the machine. Also, $v_{ti} = (2T_i/m_i)^{1/2}$ and $\rho_i = v_{ti}/|\omega_{ci}|$. For a large Shafranov shift of the flux surfaces, $\mathcal{F}$ gives a large amplification of E_r at the outer midplane. Equation (2) reproduces the core E_r in Fig. 1 to better than 30%. Note that E_r is independent of the sign of B, although profile changes can modify it. The value E_r becomes positive on open field lines since there sheath and parallel electron physics gives $\phi \sim T_e$, and T_e decays radially. Here we have focused on the poloidal variation of the classical $\mathbf{u}_{gc}$ drift in the core. It is likely that similar poloidally dependent particle fluxes can be driven by plasma turbulence [8]; these would likewise couple through the particle continuity equation to strongly affect E_r near the separatrix.

3. Cross-field drifts for double-null DIII-D and NSTX devices

Double-null magnetic configurations can reduce the peak heat flux on divertor plates by splitting the power between upper and lower divertors. However, even if the configuration is magnetically balanced, cross-field drifts can produce significant up/down plasma asymmetries in addition to the inboard/outboard asymmetry observed in single-null configurations.

We demonstrate the effect of the drifts with a UEDGE simulation of DIII-D in a balanced double-null configuration. The core-edge plasma density at the 92% flux surface is 3×10^{19} m^{-3}, the total power from the core to the SOL is 2.5 MW, and the particle recycling coefficients are 0.95 and 0.90 at the divertor plates and walls, respectively. Anomalous diffusion coefficients are 0.5 m^2/s. Plasma density and heat flux at each of the divertor plates are shown in Figs. 3 and 4, respectively. The two sets of curves refer to cases B_t in the standard ($\mathbf{u}_{gc}$ downward: solid curves) and reversed directions ($\mathbf{u}_{gc}$ upward: dashed curves). The profiles of the upper and lower divertors are just interchanged when B_t is reversed. Differences in the upper and lower divertor profiles are due entirely to cross-field drifts. The large density asymmetries in Fig. 3 can be understood as primarily from nE_r/B_t fluxes in the private-flux regions [2]; for normal B_t, these flows move particles from the lower outboard plate to the lower inner plate, and vice versa on the upper plates owing to the change in sign of E_r in the upper private-flux region. For the heat flux in Fig. 4, most of the core power goes to the outer divertor plates because of increased volume there and higher outer midplane radial fluxes from steeper gradients (via outward Shafranov-shift of flux surfaces). The up/down asymmetry in heat fluxes on the outer plates are opposite to that shown for the densities in Fig. 3. The heat-flux asymmetry is primarily caused by an excess of electrons flowing along $\mathbf{B}$ from the cooler T_e region at the upper plate to the hotter lower plate (giving a thermoelectric current from lower to upper plate). This excess electron flow convects electron thermal energy from the upper plate to the lower plate (0.2 MW in this case), yielding the heat flux asymmetry seen in Fig. 4

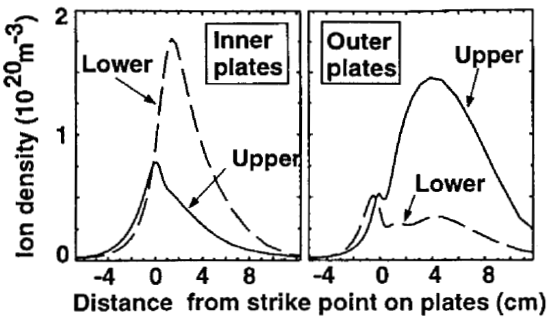

FIG. 3: Divertor plate ion density for DIII-D double-null case

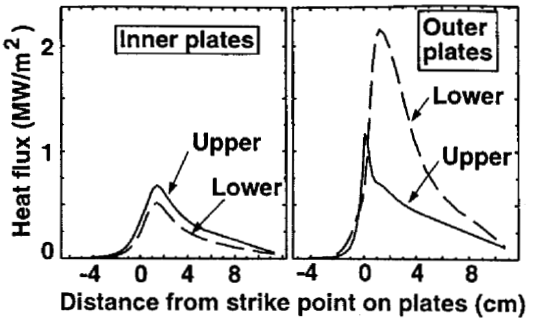

FIG. 4: Divertor plate heat flux for DIII-D double-null case

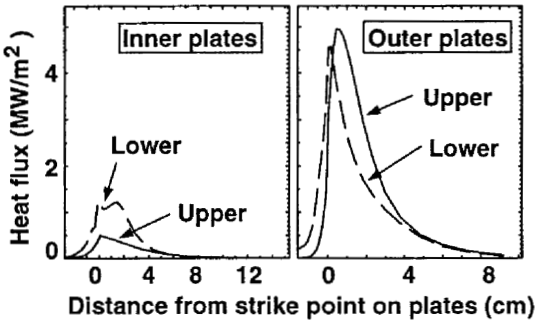

FIG. 5: Divertor plate heat flux for NSTX double-null case

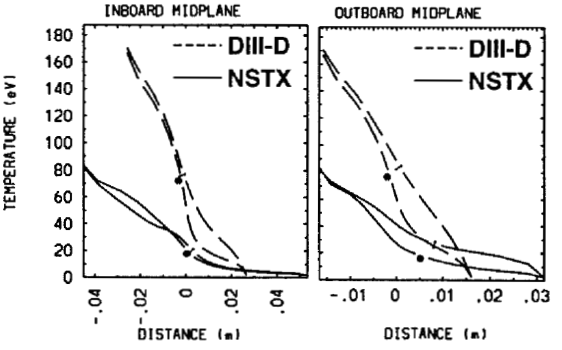

FIG. 6: Inner and outer midplane T_e and T_i profiles comparing DIII-D and NSTX cases.

To assess the relative effect of cross-drifts in conventional versus spherical tokamaks, the double-null DIII-D simulation just presented is compared to a corresponding one for NSTX. The same anomalous diffusion coefficients and boundary conditions are used, except that the power into the SOL is set at 1.5 MW for NSTX to give the same average radial heat flux at the core boundary as used for DIII-D (45 MW/m^2). These devices have similar poloidal cross-sections, but the major radius is 1.7 m in DIII-D versus 0.8 m in NSTX. Also, $B_t = 2.0$ T in DIII-D and only $B_t = 0.3$ T in NSTX, with plasma currents of 2 MA in DIII-D and 1 MA in NSTX. Figure 5 shows the heat flux on the outer plates corresponding to Fig. 4; inner plate heat fluxes are much lower. Note that for NSTX, the profiles are much more up/down symmetric. The greater symmetry arises because the parallel electron current flow for NSTX is much smaller owing to the lower SOL electron temperature. The midplane electron temperature profiles for NSTX and DIII-D are shown in Fig. 6. Even though the radial heat flux is the same, the shorter parallel connection length for NSTX results in the lower T_e because of the more rapid parallel heat conduction to the plates. For higher powers, the heat-flux asymmetry would increase for NSTX.

4. Experiment/simulation comparison for DIII-D single null

We have examined the effect of drifts in the edge and scrape-off layer plasmas of DIII-D by simulating a specific lower single-null, ohmically heated discharge with the outer strike-point positioned on the bias ring to enable simulation of the effect of biasing as well as the effect of drifts on unbiased plasmas. Simulation of biased plasmas is ongoing. We use a fixed-fraction impurity model to give the effect of radiation cooling of the divertor plasma.

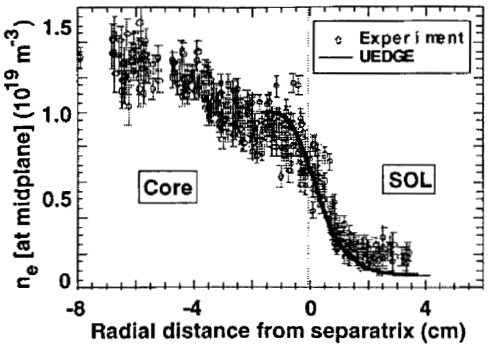

FIG. 7: DIII-D experiment/simulation comparison of midplane density profiles.

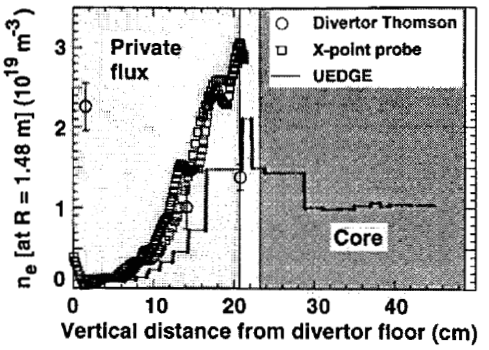

FIG. 8: DIII-D experiment/simulation comparison of divertor region density profiles.

Good agreement is obtained with measured upstream and downstream profiles of density and temperature with anomalous diffusivities of $D = 0.35$ m^2/s, and $\chi_{e,i} = 1.8$ m^2/s; midplane density is shown in Fig. 7. These diffusivities are consistent with those used in earlier simulations without drift effects [11]. The divertor region density is measured with both a divertor Thomson system, and an insertable probe. Both measurements are taken along a vertical line at line R=1.48 m which passes just on the high-field side of the X-point as shown in Fig. 8. The inner leg is detached on this discharge with $T_e \approx 1$ eV. On the outer leg, the peak $T_e \approx 30$ eV. The divertor densities are quite low, as is the upstream density. The cross-field drifts seem to have a small effect on the measurable plasma parameters for this case, decreasing the density near the inner strike point by $\sim 25\%$. The drifts do affect the poloidal flow of the deuterium plasma, and hence should affect the flow of carbon impurities originating from wall sputtering. We will study this effect with the multispecies impurity model.

5. Core-edge coupling

CORSICA 2, introduced in Ref. [12], self-consistently evolves whole-cross-section tokamak transport equations. The plasma core is time-advanced using the fully implicit 1D Grad-Hogan code CORSICA 1, and the edge and SOL are simulated with a choice of edge models, the most comprehensive of which is UEDGE. Within each time-step, the core and edges codes are run sequentially and the shared boundary conditions are iterated via a Newton scheme until self-consistency is reached. The coupled fields include n_D, T_e, T_i, n_{gas}, and the angular momentum L_z. A recent focus has been on improving consistency in the core/edge transport equations for L_z. We have also improved the coupling algorithm: The coupling surface is at the innermost core surface for UEDGE (i.e., it is where UEDGE's boundary condition is applied), but the core transport grid can extend over its full usual domain (i.e., to a surface very near the separatrix). The core-code boundary condition is then varied internally to achieve the value requested by the Newton solver at the coupling surface. This permits improved solutions for those fields which evolve under transport but are either not evolved by UEDGE, *e.g.*, q, or are not included among those coupled for a given run. It also provides a numerical test of uniform 1D overlap at the coupling surface; tests show good overlap of the two solutions.

6. ACKNOWLEDGMENTS

Work performed under the auspices of the U.S. Department of Energy by the University of California Lawrence Livermore National Laboratory under contract No. W-7405-Eng-48.

References

[1] BURRELL, K.H., Phys. Plasmas **4** (1997) 1499.

[2] ROGNLIEN, T.D., PORTER, G.D., and RYUTOV, D.D., J. Nucl. Mater. **266-269** (1999) 654.

[3] ROGNLIEN, T.D., RYUTOV, D.D., MATTOR, N., and PORTER, G.D., Phys. Plasmas **6** (1999) 1851.

[4] CHANKIN, A.V., *et al.*, Contrib. Plasma Phys. **40** (2000) 288.

[5] SCHNEIDER, R., *et al.*, Contrib. Plasma Phys. **40** (2000) 328.

[6] ROZHANSKY, V., *et al.*, Contrib. Plasma Phys. **40** (2000) 423.

[7] XU, X.Q., *et al.*, Phys. Plasmas **7** (2000) 1951.

[8] XU, X.Q., *et al.*, paper at this conference.

[9] LUXON, J.L., *et al.*, in Proc. 11^{th} Int. Conf. Plasma Phys. Controlled Nucl. Fusion (IAEA, Vienna, 1987), p. 159.

[10] PENG, M, *et al.*, Nucl. Fusion **40** spec. issue (Proc. 17*th* IAEA Fusion Eng. Conf., Yokohama, Japan, Oct. 1998) (2000) 583.

[11] PORTER, G.D., *et al.*, Phys. Plasmas **7** (2000) 3663.

[12] TARDITI, A., *et al.*, Contrib. Plasma Phys. **36** (1996) 132.